Magnesium-doped $MAPbI_3$ Perovskite Layer for Enhanced Photovoltaic Performance in Humid Air Atmosphere

*Fu Yang, Muhammad Akmal Kamarudin, Gaurav Kapil, Daisuke Hirotani, Putao Zhang, Chi Huey Ng, Tingli Ma, Shuzi Hayase**

Kyushu Institute of Technology, 204 Hibikino Wakamatsu-ku, Kitakyushu 808-0196,

KEYWORDS perovskite solar cell; Magnesium iodide; ambient atmosphere; $CH_3NH_3PbI_3$; stability; mesoporous structure.

ABSTRACT

Despite the high efficiency of $MAPbI_3$ perovskite solar cell, the long term stability and degradation in humid atmosphere are issues that still needed to be addressed. In this work, magnesium iodide (MgI_2) was first successfully used as a dopant into $MAPbI_3$ perovskite prepared in humid air atmosphere. Mg doping decreased the valence band level which was determined from photoelectron yield spectroscopy. Compared to the pristine $MAPbI_3$ perovskite film, the 1.0 % Mg doped perovskite film showed increased crystal grain size and formation of pinhole-free perovskite film. Performance of the solar cell was increased from 14.2 % of the doping-free solar cell to 17.8 %

of 1.0 % Mg doped device. Moreover, 90 % of the original PCE was still retained after storage in 30~40% relative humidity for 600 h.

INTRODUCTION

Perovskite-based solar cell was first reported by Miyasaka et al. in 2009 showing an efficiency of 3.9 %.[1] Just after several years, the efficiency significantly increased up to 22.7 % which is comparable to current silicon solar cell.[2-3] The high efficiency of lead-based perovskite solar cells can be attributed to the band gap close to the Shockley-Queisser limit, high optical absorption coefficient, excellent electron mobility and large electron diffusion length.[4-8] However, compared to single crystalline perovskite, polycrystalline perovskite material showed shorter photoluminescence lifetime, suggesting the presence of electronic defects.[9] These defects are originated from grain boundaries within the perovskite which could trap free charge carriers and thus decrease the efficiency.[10-13] The prototypical organic-inorganic perovskite, $MAPbI_3$ (MA, $CH_3NH_3^+$) has a tetragonal structure and a band gap of around 1.5 eV. Despite these excellent properties, the material is still far from being used in real application due to low stability in air and prone to degradation in humid atmosphere.[14-16] The organic cation MA is mainly responsible for the tetragonal structure stability and $MAPbI_3$ perovskite layer. And it has been reported that partial caesium or rubidium substitution of MA can effectively improve the stability because of the smaller size of inorganic cation could induce an entropic stabilisation.[17-18] The electronic properties of perovskite material are mainly determined by the Pb-site. Moreover, the chemical composition of the perovskite also determine the electrical and optical properties of the perovskite materials.[19] Therefore, partials substituting lead or doping with other metals cations can effectively modify the optoelectronic properties of perovskite materials.[20-22] Zhao et al. investigated the effect

of alkali metal doing in $MAPbI_3$ perovskite.[23] They suggested that potassium passivated the trap states in the perovskite and led to bigger grain size. Similar effect has also been observed in the case of doping with bivalent and trivalent metals, Zn^{2+}, Sb^{3+} and Sr^{2+}.[24-26] Doping of $MAPbI_3$ with Ag has also been investigated where decreased in the electron concentration and thus improved electron mobility has been cited as the factors leading to the increase in the PSC efficiency.[27] The nontoxic alkaline-earth metals of beryllium (Be, ionic radius 59 pm) magnesium (Mg, ionic radius 86 pm), calcium (Ca, ionic radius 114pm), strontium (Sr, ionic radius 132 pm), and barium (Ba, ionic radius 149 pm) are the earth abundant elements have a stable divalent oxidation state which are considered of good candidates for the replacement of toxic lead (Pb, ionic radius 132 pm). Many studies have focused on research in the energy band structure by doping the perovskite with Ba^{2+}, Sr^{2+} and Ca^{2+}.[28-30] However, rarely no experiment research of Mg^{2+} doping into the perovskite is reported. The band gap of $MAMgI_3$ is 1.39 eV that is obvious narrower than the other three metals (3.97 eV, 3.94 eV and 3.89 eV for $MABaI_3$ $MASrI_3$ and $MACaI_3$, respectively), which is approach to the band gap of $MAPbI_3$ (1.55 eV).[31] In addition, $MAMgI_3$ exhibits a strong and wide absorption at 4.5-9.5 eV in the ultraviolet spectrum region, which would be a promising material for solar cells in the region. Therefore, research in how Mg^{2+} affect into energy band structure and the morphology of the perovskite will be challenge and meaningful.

In this work, for the first time, we explored experimentally the effect of Mg doping in $MAPbI_3$ perovskite. The X-ray diffraction (XRD) analysis shows that there was no change in the crystal structure of the perovskite upon doping with Mg. Although the doping did not alter bandgap of the perovskite, from the photoelectron yield spectroscopy measurement, the valence band value became deeper. The perovskite materials were then evaluated for their photovoltaic properties and the lifetime stability was also performed at 30-40 % relative humidity (RH). The efficiency of the

solar cell was increased from 14.2 % of the doping-free solar cell to 17.8 % of 1.0 % Mg doped device. Moreover, 90 % of the original PCE was still retained after storage in 30~40% relative humidity for 600 h.

RESULTS AND DISCUSSION

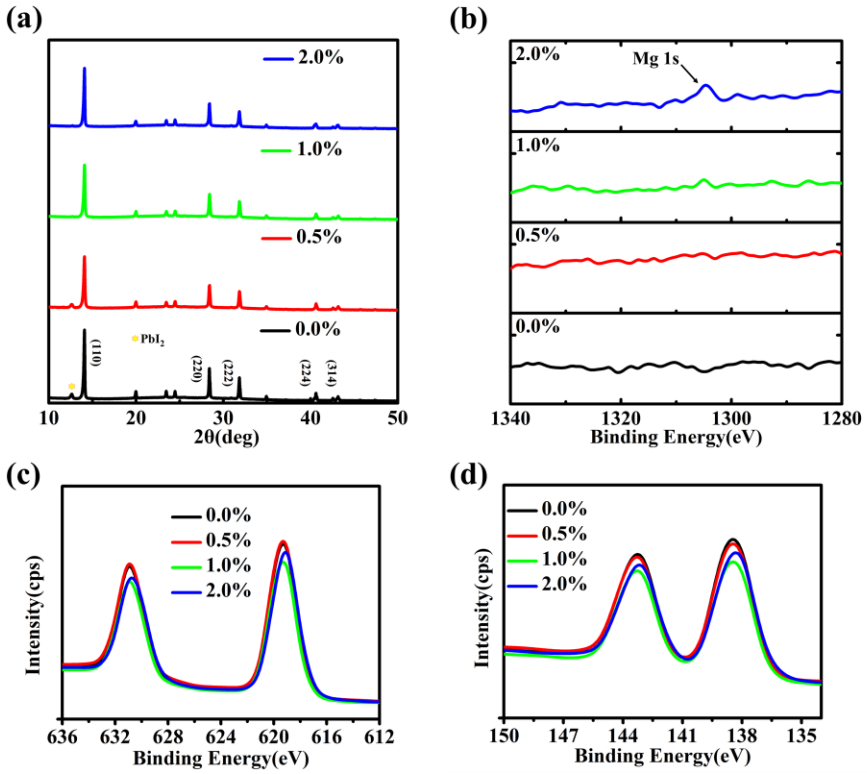

Figure 1 (a) XRD spectra of different molar ratio Mg doped $MAPbI_3$ perovskite layer on glass substrate. (b) XPS core level spectra of Mg 1s; (c) XPS core level spectra of Pb 4f; and (d) XPS core level spectra of I 3d. The XPS sample was prepared by spin-coating Mg doped $MAPbI_3$ perovskite precursor solution on 2×2 cm FTO substrates.

Figure 1a shows XRD patterns of different molar ratio Mg doped $MAPbI_3$ perovskite films (0.0 %, 0.5 %, 1.0 %, and 2.0 %). All the films were prepared on glass substrates using ethyl acetate as the anti-solvent by one-step spin-coating method at 30%~40% RH air atmosphere. Strong intensity

peaks at 14.09°, 28.42°, 31.85°, 40.63° and 43.16° were observed, which are well-oriented in (110), (220), (222), (224) and (314) directions of the $MAPbI_3$ perovskite. This is consistent with previous researches.[32-34] In addition, a weak diffraction peak appeared at 12.7° which is assigned to PbI_2, where the peak intensity decreased upon increasing Mg doping, and nearly no peak appeared when the doping ratio was more than 1.0 % which is exhibited in XRD patterns between 12.0° and 13.0° shown in Figure S1. Thelakkat et. al. proved that the rate of degradation of $CH_3NH_3PbI_3$ could be accelerated because of PbI_2 residue present in the perovskite film.[35] Moreover, researchers have proved that the surface defects and trap state density originating from uncoordinated Pb atoms of the residual PbI_2 limiting the performance of PSCs.[36] This means Mg doping into $MAPbI_3$ perovskite layer enhanced the conversion from PbI_2 to complete $MAPbI_3$ perovskite. Additionally, it also indirectly indicates that Mg doping enhanced moisture resistance of the perovskite films as it is known that $MAPbI_3$ tend to degrade into PbI_2 in the presence of water.[37-38] Hydrophobicity is another factor to confirm moisture resistance of the perovskite films. Therefore, the contact angles of the pristine and 1.0% Mg doped $MAPbI_3$ perovskite were measured and shown in Figure S4. Contact angle of the 1.0 % Mg doped MAPbI3 film is calculated to be 69.9°, which is evidently larger than that of the pristine film with 50.3°. The increase of water contact angle suggests the enhancement on water-resistance of the 1.0% Mg doped perovskite film, which is beneficial for long-term stability of the solar cells. The wide scan of X-ray photoelectron spectroscopy (XPS) of different molar ratio Mg doped $MAPbI_3$ perovskite are exhibited in Figure S2. Figure 1b shows a peak position at 1304 eV which is assigned to Mg 1s peak, and the intensity increased when increasing the Mg doping suggesting that Mg is successfully doped into the $MAPbI_3$ structure.[39] Figure 1c, d shows the Pb 4f and I 3d core levels which indicate the I/Pb surface atomic ratio are close to 3 in all the films. Moreover, the Pb 4f and I 3d peaks move to lower binding energy when

increasing the Mg doping content, suggesting a change in the oxidation state of Pb and I with the addition of MgI_2.[40]

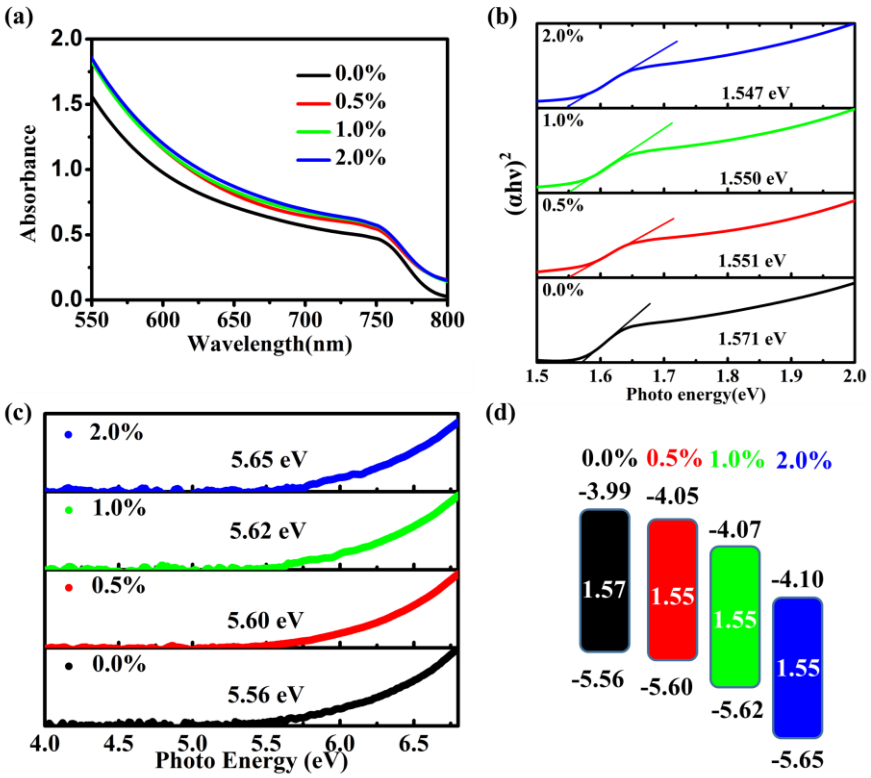

Figure 2 (a) UV-vis spectra of different Mg doped $MAPbI_3$ perovskite films on glass substrates. (b) $(ahv)^2$ versus energy. (c) PESA measurement of different Mg doped perovskite films on FTO glass substrates and (d) The corresponding energy diagram.

Figure 2a shows the UV-vis absorption spectra of different molar ratio Mg doped $MAPbI_3$ perovskite layers. It is obviously that the absorbance of Mg doped perovskite layer increased compared to pristine $MAPbI_3$ film. The increased absorbance can be attributed to better surface coverage and pinhole-free morphology of the perovskite layer.[41] The band gaps are calculated from Tauc plot are shown in Figure 2b. The optical band gap decreased marginally from 1.571 eV for pure $MAPbI_3$ perovskite to 1.547 eV for 2.0% Mg doping. Photoelectron yield spectroscopy (PYS)

was utilized to measure the valence band of the perovskite materials.[42-44] The valence band edge of the perovskite films showed a clear decreasing trend after incorporation of Mg into $MAPbI_3$ perovskite, as determined by photoelectron spectroscopy in air, shown in Figure 2c. The valence band edge shifted from -5.56 eV of $MAPbI_3$ to more negative values of -5.60 eV, -5.62 eV and -5.65 eV for 0.5 %, 1.0 % and 2.0 % Mg doping, respectively. Based on the above results, the energy diagram upon Mg doping is given in Figure 2d. The valence electron of lead and magnesium is $5d^{10}/6s^2/6p^2$ and $2s^2/2p^6/3s^2$, respectively. When Mg was added to the perovskite, the carrier transition was changed from Mg 1p—Mg 1s of the pristine MgI_2 to the Mg 1d—Mg 1s of the doped perovskite, which is shown in Figure S8. For the Mg doped $MAPbI_3$, the valence bands are mostly occupied by the p orbitals of iodide atoms, and the conduction bands contain of a large proportion of the s orbitals of Magnesium atoms and the p orbitals of the lead atoms.[45] It is clearly shown in Figure 2d that the electronic configuration of $MAPbI_3$ suffers only minor changes after incorporation of low content of MgI_2, which is critical in order to retain the high photovoltaic performance of $MAPbI_3$ perovskite materials.[46] In addition, the time-resolved photoluminescence (TRPL) spectra of the controlled and 1.0% Mg doped perovskite film are displayed in Figure S7. The PL decay times are obvious increased from τ_{ave} of 150.39 ns for the pristine $MAPbI_3$ perovskite film to the 347.63 ns for the 1.0% Mg doped perovskite film, which indicates that Mg doping enhances the carrier lifetime.[47]

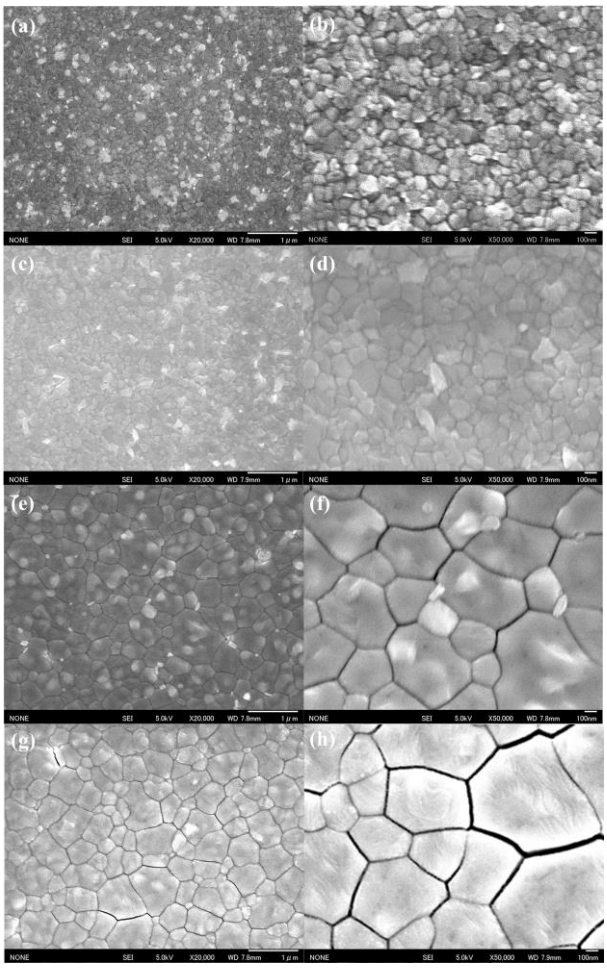

Figure 3 Top view SEM images of the different Mg doped MAPbI3 perovskite layers on FTO/compact TiO_2/Mesoporous TiO_2 substrates. (a) (b) 0.0%; (c) (d) 0.5%; (e) (f) 1.0%; (g) (h) 2.0%. Scale bar for (a) (c) (e) (g) is 1μm and (b) (d) (f) (h) is 100 nm.

Figure 3 shows the top-view morphology of the different molar ratio Mg doped $MAPbI_3$ perovskite layers observed by scanning electron microscopy (SEM). It can be calculated that the average grain size is around 110 nm of pristine $MAPbI_3$ film, 190 nm for 0.5 %, 580 nm for 1.0 % and 600 nm of 2.0 % Mg doped sample. It is clear the grain size gradually increased when increasing the doping content from 0.0 % to 2.0 %. However, 2.0% Mg doped film showed cracks and especially

significant for the 4.0% Mg doped as shown in Figure S5. The cracks have been reported to be mainly caused by the mechanical stress because of the fast growth rate of perovskite film during annealing step.[48] The grain size is one of the governing parameters for determining the diffusion length and the charge carrier recombination rate.[49] Small grain size directly correlates to large number of grain boundaries in the perovskite layer. Not only these sites act as charge trap sites, but also they are prone to attack by water molecules and these will accelerate degradation of the perovskite.

During the growth process of perovskite layer, the growth rate of crystal grain is determined by the Gibbs free energy. The relationship between the nucleus radius (r) and overall Gibbs free energy change (ΔG) can be derived from the equation[50]

$$\Delta G(r) = -\frac{4\pi r^3}{3V_M} RT \ln(S) + 4\pi r^2 \gamma$$

Where V_M, γ, S, R, and T represent nucleus` molar volume, energy of liquid-crystalline nucleus interface, supersaturation ratio, absolute temperature and gas constant, respectively. Figure S 9a and 9b schematically describe the Gibbs free energy diagrams as a function of nuclei radius in case of MgI_2 doping. Doping Mg into the perovskite can increse the Gibbs free energy owning to the effect of chemical heterogeneity.[32, 51] As a result, less nucleis are formed, inducing the bigger grain size. On the other hand, the coordination interaction between $CH_3NH_3^+$ and Mg^{2+} is higher than that of $CH_3NH_3^+$ and Pb^{2+}, which results in the electron cloud become more closer between $CH_3NH_3^+$ and Mg^{2+} metal ion, which also affects the crystallization of the perovskite film.[52-53] Therefore, the stronger coordination function with organic groups, along with a higher chemical interaction between Mg^{2+} and anions, which could make the Mg doped perovskite layer prefer to grow bigger grain sizes.

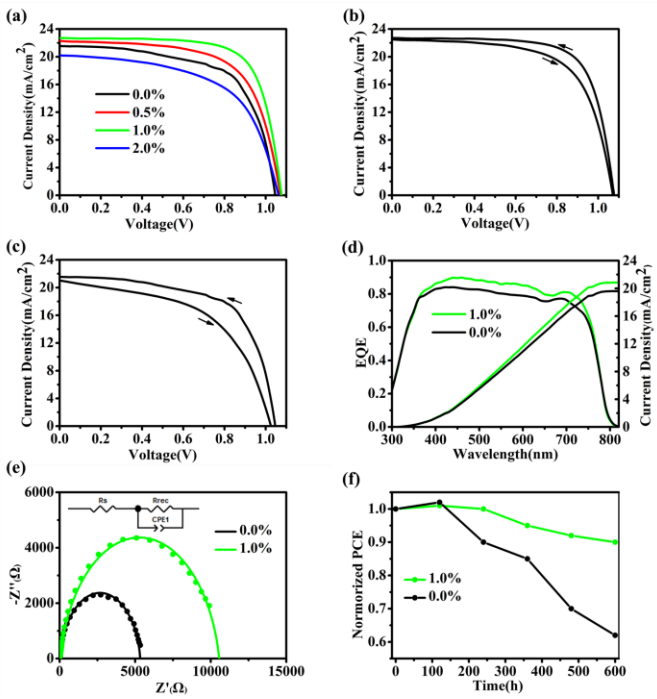

Figure 4 (a) The J−V curves of different molar ratio Mg doped $MAPbI_3$ perovskite solar cells measured under AM 1.5 solar illumination (100 mW•cm^{-2}) in air. The scanning direction is from open-circuit voltage to short-circuit current (reverse). (b) J−V curves of 1.0% Mg doped perovskite solar cell under reverse and forward voltage scans. (c) J−V curves of pristine $MAPbI_3$ perovskite solar cell under reverse and forward voltage scans. (d) EQE spectra of the pristine and 1.0% Mg doped perovskite solar cells measured in air. (e) Nyquist plots along with the equivalent circuit diagram of pristine and 1.0 % Mg doped perovskite solar cells measured at 0.7 V applied bias under dark condition. Solid lines are the fitted curves and the experimental data are shown as points. (f) The stability of pristine and 1.0% Mg doped perovskite solar cells. Devices were prepared without sealing and were kept under dark at 30~40% RH atmosphere.

The effect of different molar ratio Mg doped perovskite on solar cells performance was investigated with solar cells having the structure of FTO/Compact TiO_2/Mesoporous TiO_2/Perovskite/Spiro/Au. Devices were fabricated at 30~40% RH atmosphere. The pristine

device measured on the reverse direction has PCE of 14.5 %, short-circuit current density (J_{sc}) of 21.56 mA/cm^2, open-circuit voltage (V_{oc}) of 1.05 V, and fill factor (FF) of 64.5 %. All the photovoltaic parameters increased upon doping with Mg as shown in Figure 4a. The 1.0% Mg doped device measured on the reverse scan has a PCE of 17.8 %, along with J_{sc} of 22.72 mA/cm^2, V_{oc} of 1.08 V and FF of 72.3 %. However, 2.0 % Mg doped device showed low performance with PCE of 12.8 % which could be explained by the obvious cracks on the perovskite film (Figure 3 g, h).

The defect states and band bending always affects the hysteresis of the J-V curves which is a significant problem for conforming the actual PCE. Hence, to compare the quality of the PSCs, the hysteresis index values are calculated from the measured current-density-voltage curves.[51] The hysteresis index value of 1.0 % Mg doped perovskite device is 0.11 which is lower than that of pristine device (0.27). The lower hysteresis index could be owning to the big grain size and uniform growth of the perovskite layer, effectively reducing the grain boundaries and make the charge transfer more efficiently between grains. Figure 4d shows the IPCE curve and the corresponding calculated short-circuit current. 1.0 % Mg doped perovskite device showed higher EQE curve than the pristine device which is attributed to higher absorbance intensity of the 1.0 % Mg doped perovskite film. Electrochemical impedance spectroscopy was performed to investigate the charge transfer mechanism on the interfaces. Figure 4e shows the Nyquist plots of the pristine and 1.0% Mg doped PSCs measured under dark condition with a bias of 0.7 V. Rs, Rrec and CPE are the sheet resistance, recombination resistance and constant phase element, respectively. As it is known that lower Rs suggests a better electro transport and larger Rrec implies the lower recombination rate.[44] From the fitting, Rrec increased from 5303 Ω to 10545 Ω after 1.0 % MgI_2 has been incorporated, suggesting the recombination rate is decreased.[24] Therefore, it can be concluded that

the larger Rrec of 1.0 % Mg doped perovskite based device indicates that the carrier mobility in correspondent device is improved thus leading to enhanced V_{oc} and FF. Furthermore, air stability of pristine and 1.0 % Mg doped PSCs were evaluated which was shown in Figure 4f. All the devices prepared without encapsulation was stored at room temperature at 30~40% RH atmosphere. After 600 h, the efficiency of pristine device decreased to 60 % of its initial value. However, the 1.0 % Mg doped device showed excellent stability in high humidity condition where 90 % of the original PCE was still retained. The more stable Mg doped perovskite device is possible reason for the stability of the Mg doped perovskite layer as proved by the perovskite film stability test shown in Figure S6. It is clear from Figure S6 that the 1.0 % Mg doped perovskite layer was stable as the UV absorbance showed nearly no decrease after two weeks while the pristine film showed significant decrease.

CONCLUSION

In conclusion, we have successfully doped Mg into $MAPbI_3$ without altering the crystal structure. The MgI_2 doping resulted in lower conduction and valence band, perfectly matching with the conduction band of TiO_2 and valence band of spiro-OMeTAD. Higher quality perovskite films with bigger grain and pin-hole free was obtained upon Mg doping. For pristine device, the efficiency was 14.2 % compared to 17.8 % for 1 % Mg doped sample. Moreover, the PCE only dropped 10% after storage in 30~40 % relative humidity for 600 h. Our results suggest that doping Mg into perovskite layer is a good strategy to enhance stability and the photovoltaic performance of the perovskite solar cells.

EXPERIEMNTAL SECTION

Preparation of perovskite solar cells

Fluorine-doped tin oxide (FTO glass, Nippon Sheet Glass Co. Ltd) substrates were etched with r hydrochloric acid solution and zinc powder. The titanium dioxide compact layer was spin-coated 0.15 M titanium diisopropoxide bis(acetyacetonate) (75 wt% in isopropanol, Aldrich) in 1-butanol (99.8 %, Aldrich) on an the FTO substrate at 2000 rpm for 30 seconds. Then the substrate was heated at 125 ^{o}C for 5 min. Next, the titanium dioxide paste (Dyesol 30NRD, diluted in ethanol at 1:4 weight ratio) was spin-coated at 500 rpm 5s and 5000 rpm for 30 s. After drying at 125 ℃ for 30 min, the substrate was annealed at 500 ℃ for 30 min. The perovskite solution was prepared by dissolving 239 mg MAI (TCI, 98 %) and 692mg PbI_2 (TCI, 99.99 %) into 0.2 mL dimethyl sulfoxide (DMSO, Aldrich, 99.8 %) and 0.8 mL dimethylformamide (DMF, Aldrich, 99.8 %) to achieve 1.5 M $MAPbI_3$ perovskite precursor solution. For preparing the Mg doped perovskite precursor solution, adding the proper ratio of MgI_2 (99.998 %, Aldrich) into the 1.5 M $MAPbI_3$ perovskite precursor solution. The Spiro-MeOTAD solution was prepared by mixing 72.3 mg Spiro-MeOTAD (Aldrich, 99 %), 29 μL FK209 (Aldrich, 99 %) (300 mg/mL in acetonitrile), 7.5 μL Li-TFSI (Aldrich, 99.95 %) (520 mg/mL in acetonitrile) and 28.8μL tert-butylpyridine (Aldrich, 96 %) in 1 mL chlorobenzene solution. The perovskite layer was prepared on the mesoporous TiO_2 substrate by adding 0.1 mL perovskite precursor solution and spin-coated at 4000 rpm for 25 s. 0.5 mL ethyl acetate (99.8 %, Aldrich) antisolvent was dripped during the spin-coated progress.[54] The spin-coated perovskite film was annealed at 100 ℃ for 10 min. The Spiro -MeOTAD layer spin-coated on the perovskite layer at 4000 rpm for 30 s. Finally, Au electrode with 80 nm thickness was deposited on the Spiro film by thermal evaporation.

Device Characterization

Current-density-voltage curves of the perovskite solar cells with a 0.10 cm^2 exposure area were measured under AM 1.5G 100 $mWcm^{-2}$ irradiation uing a solar simulator (CEP-2000SRR, Bunkoukeiki Inc.,). UV-Vis spectra was obtained with a UV/Vis spectrophotometer (JASCO V-670). The scanning electron microscope (JEOL, Neoscope, JSM-6700F) was used to measure morphologies of perovskite layer. The EQE spectra were recorded using a Xenon lamp, a potentiostat and a monochromator (Bunkouki CEP-2000SRR). XRD patterns were obtained by the monochromatic Cu-Kβ irradiation with a X-ray diffractometer (Rigaku Smartlab, 45 kV/200 mA). Photoelectron yield spectroscopy (PYS) was used to determine the valence band using a Bunkoukeiki KV205-HK ionization energy measurement system with – 5.0 V of applied voltage under 10^{-4} Pa vacuum. Electrochemical impedance spectroscopic measurements were tested with a frequency range from 1 Hz to 1 MHz at 0.7 V applied bias under dark condition.

ASSOCIATED CONTENT

Supporting Information.

Additional data and results (XRD, XPS, Contact angle, SEM images, UV-vis spectra of perovskite film, Time-resolved photoluminescence spectra, DOS diagrams, Gibbs free energy diagram for nucleation) (PDF)

AUTHOR INFORMATION

Corresponding Author

* Email: hayase@life.kyutech.ac.jp.

Present Addresses

† 2-4 Hibikino, Wakamatsu-ku, Kitakyushu 808-0196, Japan

Notes

There are no conflicts to declare.

Funding Sources

This research was supported by Core Research for Evolutional Science and Technology

(CREST) project of Japan Science and Technology

REFERENCES

(1) Kojima, A.; Teshima, K.; Shirai, Y.; Miyasaka, T. Organometal Halide Perovskites as Visible-Light Sensitizers for Photovoltaic Cells. *Journal of the American Chemical Society* **2009,** *131* (17), 6050-6051.
(2) Domanski, K.; Alharbi, E. A.; Hagfeldt, A.; Grätzel, M.; Tress, W. Systematic Investigation of the Impact of Operation Conditions on the Degradation Behaviour of Perovskite Solar Cells. *Nature Energy* **2018**, 3(1), 61–67.
(3) Yang, W. S.; Park, B.-W.; Jung, E. H.; Jeon, N. J.; Kim, Y. C.; Lee, D. U.; Shin, S. S.; Seo, J.; Kim, E. K.; Noh, J. H. Iodide Management in Formamidinium-Lead-Halide–Based Perovskite Layers for Efficient Solar Cells. *Science* **2017,** *356* (6345), 1376-1379.
(4) Lee, M. M.; Teuscher, J.; Miyasaka, T.; Murakami, T. N.; Snaith, H. J. Efficient Hybrid Solar Cells Based on Meso-Superstructured Organometal Halide Perovskites. *Science* **2012,** *338* (6107), 643-647.
(5) Liu, M.; Johnston, M. B.; Snaith, H. J. Efficient Planar Heterojunction Perovskite Solar Cells by Vapour Deposition. *Nature* **2013,** *501* (7467), 395-398.
(6) Zhou, H.; Chen, Q.; Li, G.; Luo, S.; Song, T.-b.; Duan, H.-S.; Hong, Z.; You, J.; Liu, Y.; Yang, Y. Interface Engineering of Highly Efficient Perovskite Solar Cells. *Science* **2014,** *345* (6196), 542-546.
(7) Stranks, S. D.; Eperon, G. E.; Grancini, G.; Menelaou, C.; Alcocer, M. J.; Leijtens, T.; Herz, L. M.; Petrozza, A.; Snaith, H. J. Electron-Hole Diffusion Lengths Exceeding 1 Micrometer in an Organometal Trihalide Perovskite Absorber. *Science* **2013,** *342* (6156), 341-344.
(8) Shockley, W.; Queisser, H. J. Detailed Balance Limit of Efficiency of p-n Junction Solar Cells. *Journal of applied physics* **1961,** *32* (3), 510-519.
(9) Shao, Y.; Fang, Y.; Li, T.; Wang, Q.; Dong, Q.; Deng, Y.; Yuan, Y.; Wei, H.; Wang, M.; Gruverman, A. Grain Boundary Dominated Ion Migration in Polycrystalline Organic–Inorganic Halide Perovskite Films. *Energy & Environmental Science* **2016,** *9* (5), 1752-1759.
(10) Yang, M.; Zeng, Y.; Li, Z.; Kim, D. H.; Jiang, C.-S.; van de Lagemaat, J.; Zhu, K. Do Grain Boundaries Dominate Non-Radiative Recombination in CH 3NH3PbI3 Perovskite Thin Films? *Physical Chemistry Chemical Physics* **2017,** *19* (7), 5043-5050.
(11) Sherkar, T. S.; Momblona, C.; Gil-Escrig, L. n.; Ávila, J.; Sessolo, M.; Bolink, H. J.; Koster, L. J. A. Recombination in Perovskite Solar Cells: Significance of Grain Boundaries, Interface Traps, and Defect Ions. *ACS energy letters* **2017,** *2* (5), 1214-1222.

(12) Fei, C.; Li, B.; Zhang, R.; Fu, H.; Tian, J.; Cao, G. Highly Efficient and Stable Perovskite Solar Cells Based on Monolithically Grained CH3NH3PbI3 Film. *Advanced Energy Materials* **2017,** *7* (9).
(13) Niu, T.; Lu, J.; Munir, R.; Li, J.; Barrit, D.; Zhang, X.; Hu, H.; Yang, Z.; Amassian, A.; Zhao, K. Stable High‐Performance Perovskite Solar Cells via Grain Boundary Passivation. *Advanced Materials* **2018,** *30*, 1706576..
(14) Tai, Q.; You, P.; Sang, H.; Liu, Z.; Hu, C.; Chan, H. L.; Yan, F. Efficient and Stable Perovskite Solar Cells Prepared in Ambient Air Irrespective of the Humidity. *Nature communications* **2016,** *7*, 11105.
(15) Troughton, J.; Hooper, K.; Watson, T. M. Humidity Resistant Fabrication of CH3NH3PbI3 Perovskite Solar Cells and Modules. *Nano Energy* **2017,** *39*, 60-68.
(16) Han, Y.; Meyer, S.; Dkhissi, Y.; Weber, K.; Pringle, J. M.; Bach, U.; Spiccia, L.; Cheng, Y.-B. Degradation Observations of Encapsulated Planar CH3NH3PbI3 Perovskite Solar Cells at High Temperatures and Humidity. *Journal of Materials Chemistry A* **2015,** *3* (15), 8139-8147.
(17) Saliba, M.; Matsui, T.; Domanski, K.; Seo, J.-Y.; Ummadisingu, A.; Zakeeruddin, S. M.; Correa-Baena, J.-P.; Tress, W. R.; Abate, A.; Hagfeldt, A. Incorporation of Rubidium Cations into Perovskite Solar Cells Improves Photovoltaic Performance. *Science* **2016,** *354* (6309), 206-209.
(18) Conings, B.; Drijkoningen, J.; Gauquelin, N.; Babayigit, A.; D'Haen, J.; D'Olieslaeger, L.; Ethirajan, A.; Verbeeck, J.; Manca, J.; Mosconi, E. Intrinsic Thermal Instability of Methylammonium Lead Trihalide Perovskite. *Advanced Energy Materials* **2015,** *5* (15).
(19) Gottesman, R.; Zaban, A. Perovskites for Photovoltaics in the Spotlight: Photoinduced Physical Changes and Their Implications. *Accounts of Chemical Research* **2016,** *49* (2), 320-329.
(20) Klug, M. T.; Osherov, A.; Haghighirad, A. A.; Stranks, S. D.; Brown, P. R.; Bai, S.; Wang, J. T.-W.; Dang, X.; Bulović, V.; Snaith, H. J. Tailoring Metal Halide Perovskites Through Metal Substitution: Influence on Photovoltaic and Material Properties. *Energy & Environmental Science* **2017,** *10* (1), 236-246.
(21) Lu, K.; Lei, Y.; Qi, R.; Liu, J.; Yang, X.; Jia, Z.; Liu, R.; Xiang, Y.; Zheng, Z. Fermi Level Alignment by Copper Doping for Efficient ITO/Perovskite Junction Solar Cells. *Journal of Materials Chemistry A* **2017,** *5* (48), 25211-25219.
(22) Jahandar, M.; Heo, J. H.; Song, C. E.; Kong, K.-J.; Shin, W. S.; Lee, J.-C.; Im, S. H.; Moon, S.-J. Highly Efficient Metal Halide Substituted CH3NH3I (PbI2) 1− X (CuBr2) X Planar Perovskite Solar Cells. *Nano Energy* **2016,** *27*, 330-339.
(23) Zhao, W.; Yao, Z.; Yu, F.; Yang, D.; Liu, S. F. Alkali Metal Doping for Improved CH3NH3PbI3 Perovskite Solar Cells. *Advanced Science* **2018,** *5* (2), 1700131.
(24) Jin, J.; Li, H.; Chen, C.; Zhang, B.; Xu, L.; Dong, B.; Song, H.; Dai, Q. Enhanced Performance of Perovskite Solar Cells with Zinc Chloride Additives. *ACS applied materials & interfaces* **2017,** *9* (49), 42875-42882.
(25) Zhang, J.; Shang, M.-h.; Wang, P.; Huang, X.; Xu, J.; Hu, Z.; Zhu, Y.; Han, L. n-Type Doping and Energy States Tuning in CH3NH3Pb1–x Sb2 x/3I3 Perovskite Solar Cells. *ACS Energy Letters* **2016,** *1* (3), 535-541.
(26) Shai, X.; Zuo, L.; Sun, P.; Liao, P.; Huang, W.; Yao, E.-P.; Li, H.; Liu, S.; Shen, Y.; Yang, Y. Efficient Planar Perovskite Solar Cells Using Halide Sr-Substituted Pb Perovskite. *Nano Energy* **2017,** *36*, 213-222.

(27) Chen, Q.; Chen, L.; Ye, F.; Zhao, T.; Tang, F.; Rajagopal, A.; Jiang, Z.; Jiang, S.; Jen, A. K.-Y.; Xie, Y. Ag-Incorporated Organic–Inorganic Perovskite Films and Planar Heterojunction Solar Cells. *Nano letters* **2017,** *17* (5), 3231-3237.
(28) Lu, C.; Zhang, J.; Hou, D.; Gan, X.; Sun, H.; Zeng, Z.; Chen, R.; Tian, H.; Xiong, Q.; Zhang, Y. Calcium Doped MAPbI3 with Better Energy State Alignment in Perovskite Solar Cells. *Applied Physics Letters* **2018,** *112* (19), 193901.
(29) Zhang, H.; Shang, M.-h.; Zheng, X.; Zeng, Z.; Chen, R.; Zhang, Y.; Zhang, J.; Zhu, Y. Ba^{2+} Doped CH3NH3PbI3 to Tune the Energy State and Improve the Performance of Perovskite Solar Cells. *Electrochimica Acta* **2017,** *254*, 165-171.
(30) Pérez-del-Rey, D.; Forgács, D.; Hutter, E. M.; Savenije, T. J.; Nordlund, D.; Schulz, P.; Berry, J. J.; Sessolo, M.; Bolink, H. J. Strontium Insertion in Methylammonium Lead Iodide: Long Charge Carrier Lifetime and High Fill-Factor Solar Cells. *Advanced Materials* **2016,** *28* (44), 9839-9845.
(31) Ali, R.; Hou, G.-J.; Zhu, Z.-G.; Yan, Q.-B.; Zheng, Q.-R.; Su, G. Predicted Lead-Free Perovskites for Solar Cells. *Chemistry of Materials* **2018,** *30*(3), 718-728.
(32) Fu, Y.; Akmal, K. M.; PuTao, Z.; Gaurav, K.; Tingli, M.; Shuzi, H. Enhanced Crystallization by Methanol Additive in Anti-solvent for Achieving High-quality MAPbI3 Perovskite Films in Humid Atmosphere. *ChemSusChem* 2018, DOI: doi:10.1002/cssc.201800625.
(33) Sun, S.; Salim, T.; Mathews, N.; Duchamp, M.; Boothroyd, C.; Xing, G.; Sum, T. C.; Lam, Y. M. The Origin of High Efficiency in Low-Temperature Solution-Processable Bilayer Organometal Falide Hybrid Solar Cells. *Energy & Environmental Science* **2014,** *7* (1), 399-407.
(34) Baikie, T.; Fang, Y.; Kadro, J. M.; Schreyer, M.; Wei, F.; Mhaisalkar, S. G.; Graetzel, M.; White, T. J. Synthesis and Crystal Chemistry of the Hybrid Perovskite (CH3NH3)PbI3 for solid-state sensitised solar cell applications. *Journal of Materials Chemistry A* **2013,** *1* (18), 5628-5641.
(35) Gujar, T. P.; Unger, T.; Schönleber, A.; Fried, M.; Panzer, F.; van Smaalen, S.; Köhler, A.; Thelakkat, M. The role of PbI2 in CH3NH3PbI3 Perovskite Stability, Solar Cell Parameters and Device Degradation. *Physical Chemistry Chemical Physics* **2018,** *20* (1), 605-614.
(36) Zheng, X.; Chen, B.; Dai, J.; Fang, Y.; Bai, Y.; Lin, Y.; Wei, H.; Zeng, X. C.; Huang, J. Defect Passivation in Hybrid Perovskite Solar Cells Using Quaternary Ammonium Halide Anions and Cations. *Nature Energy* **2017,** *2* (7), 17102.
(37) Kim, B. J.; Kim, D. H.; Lee, Y.-Y.; Shin, H.-W.; Han, G. S.; Hong, J. S.; Mahmood, K.; Ahn, T. K.; Joo, Y.-C.; Hong, K. S. Highly Efficient and Bending Durable Perovskite Solar Cells: Toward a Wearable Power Source. *Energy & Environmental Science* **2015,** *8* (3), 916-921.
(38) Habisreutinger, S. N.; Leijtens, T.; Eperon, G. E.; Stranks, S. D.; Nicholas, R. J.; Snaith, H. J. Carbon Nanotube/Polymer Composites as a Highly Stable Hole Collection Layer in Perovskite Solar Cells. *Nano letters* **2014,** *14* (10), 5561-5568.
(39) Yamada, Y.; Miura, M.; Tajima, K.; Okada, M.; Yoshimura, K. Pd Distribution of Switchable Mirrors Based on Mg–Y Alloy Thin Films. *Solar Energy Materials and Solar Cells* **2014,** *120*, 631-634.
(40) Cai, Q.; Li, H.; Jiang, Y.; Tu, L.; Ma, L.; Wu, X.; Yang, S.-e.; Shi, Z.; Zang, J.; Chen, Y. High-Efficiency Perovskite Solar Cells Based on MAI(PbI2)1−x(FeCl2)x Absorber Layers. *Solar Energy* **2018,** *159*, 786-793.
(41) Ren, Y.-K.; Ding, X.-H.; Wu, Y.-H.; Zhu, J.; Hayat, T.; Alsaedi, A.; Xu, Y.-F.; Li, Z.-Q.; Yang, S.-F.; Dai, S.-Y. Temperature-Assisted Rapid Nucleation: a Facile Method to Optimize

the Film Morphology for Perovskite Solar Cells. *Journal of Materials Chemistry A* **2017,** *5* (38), 20327-20333.
(42) Ito, N.; Kamarudin, M. A.; Hirotani, D.; Zhang, Y.; Shen, Q.; Ogomi, Y.; Iikubo, S.; Minemoto, T.; Yoshino, K.; Hayase, S. Mixed Sn–Ge Perovskite for Enhanced Perovskite Solar Cell Performance in Air. *The journal of physical chemistry letters* **2018,** *9* (7), 1682-1688.
(43) Ristein, J.; Stein, W.; Ley, L. Defect Spectroscopy and Determination of the Electron Diffusion Length in Single Crystal Diamond by Total Photoelectron Yield Spectroscopy. *Physical review letters* **1997,** *78* (9), 1803.
(44) Guo, Y.; Liu, C.; Inoue, K.; Harano, K.; Tanaka, H.; Nakamura, E. Enhancement in The Efficiency of an Organic–Inorganic Hybrid Solar Cell with a Doped P3HT Hole-Transporting Layer on a Void-Free Perovskite Active Layer. *Journal of Materials Chemistry A* **2014,** *2* (34), 13827-13830.
(45) Zhang, Y.; Feng, J. CH3NH3Pb1− x Mg x I3 Perovskites as Environmentally Friendly Photovoltaic Materials. *AIP Advances* **2018,** *8* (1), 015218.
(46) Lu, J.; Jiang, L.; Li, W.; Li, F.; Pai, N. K.; Scully, A. D.; Tsai, C. M.; Bach, U.; Simonov, A. N.; Cheng, Y. B. Diammonium and Monoammonium Mixed‐Organic‐Cation Perovskites for High Performance Solar Cells with Improved Stability. *Advanced Energy Materials* **2017,** *7* (18).
(47) Shi, D.; Adinolfi, V.; Comin, R.; Yuan, M.; Alarousu, E.; Buin, A.; Chen, Y.; Hoogland, S.; Rothenberger, A.; Katsiev, K. Low Trap-State Density and Long Carrier Diffusion in Organolead Trihalide Perovskite Single Crystals. *Science* **2015,** *347* (6221), 519-522.
(48) Qiu, W.; Merckx, T.; Jaysankar, M.; de la Huerta, C. M.; Rakocevic, L.; Zhang, W.; Paetzold, U.; Gehlhaar, R.; Froyen, L.; Poortmans, J. Pinhole-Free Perovskite Films for Efficient Solar Modules. *Energy & Environmental Science* **2016,** *9* (2), 484-489.
(49) Kim, H. D.; Ohkita, H.; Benten, H.; Ito, S. Photovoltaic Performance of Perovskite Solar Cells with Different Grain Sizes. *Advanced materials* **2016,** *28* (5), 917-922.
(50) Zhou, Y.; Game, O. S.; Pang, S.; Padture, N. P. Microstructures of Organometal Trihalide Perovskites for Solar Cells: Their Evolution from Solutions and Characterization. *The journal of physical chemistry letters* **2015,** *6* (23), 4827-4839.
(51) Wang, K.; Shi, Y.; Li, B.; Zhao, L.; Wang, W.; Wang, X.; Bai, X.; Wang, S.; Hao, C.; Ma, T. Amorphous Inorganic Electron‐Selective Layers for Efficient Perovskite Solar Cells: Feasible Strategy Towards Room‐Temperature Fabrication. *Advanced Materials* **2016,** *28* (9), 1891-1897.
(52) Chen, R.; Hou, D.; Lu, C.; Zhang, J.; Liu, P.; Tian, H.; Zeng, Z.; Xiong, Q.; Hu, Z.; Zhu, Y. Zinc ion as Effective Film Morphology Controller in Perovskite Solar Cells. *Sustainable Energy & Fuels* **2018,** *2* (5), 1093-1100.
(53) Chan, S.-H.; Wu, M.-C.; Lee, K.-M.; Chen, W.-C.; Lin, T.-H.; Su, W.-F. Enhancing Perovskite Solar Cell Performance and Stability by Doping Barium in Methylammonium Lead Halide. *Journal of Materials Chemistry A* **2017,** *5* (34), 18044-18052.
(54) Yang, F.; Kapil, G.; Zhang, P.; Hu, Z.; Kamarudin, M. A.; Ma, T.; Hayase, S. Dependence of Acetate-Based Antisolvents for High Humidity Fabrication of CH3NH3PbI3 Perovskite Devices in Ambient Atmosphere. *ACS Applied Materials & Interfaces* **2018,** *10* (19), 16482-16489.

TOC GRAPHICS

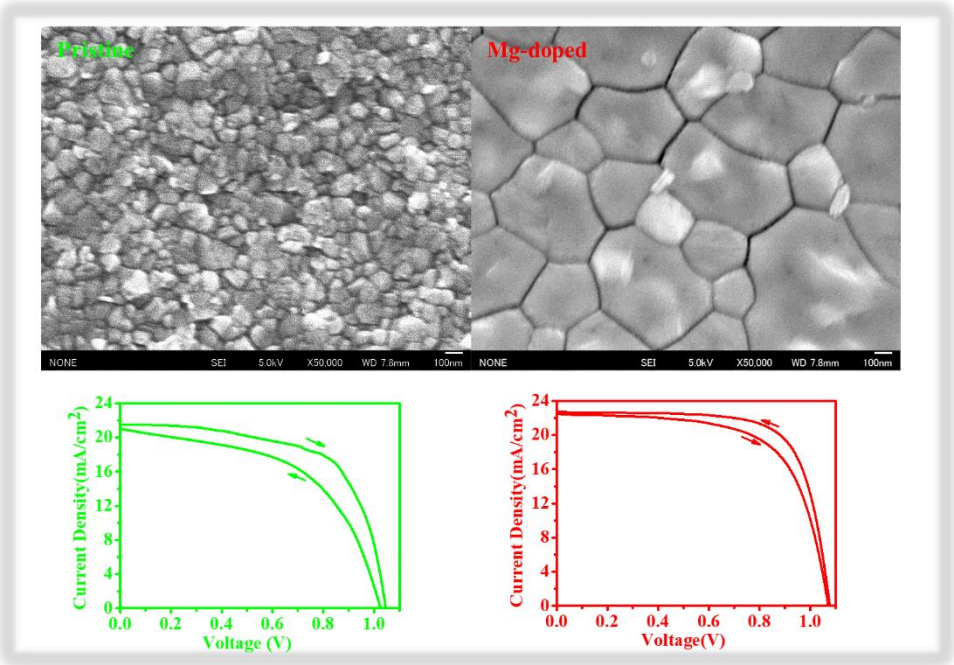

Magnesium-doped $MAPbI_3$ Perovskite Layer for Enhanced Photovoltaic Performance in Humid air atmosphere

Fu Yang, Muhammad Akmal Kamarudin, Gaurav Kapil, Daisuke Hirotani, Putao Zhang, Chi Huey Ng, Tingli Ma, Shuzi Hayase*

Kyushu Institute of Technology, 2-4 Hibikino Wakamatsu-ku, Kitakyushu 808-0196, Japan.

Email: hayase@life.kyutech.ac.jp.

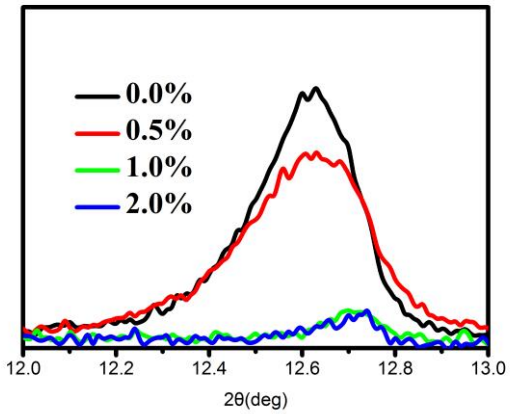

Figure S1 The Zoomed XRD peak of PbI_2 pattern.

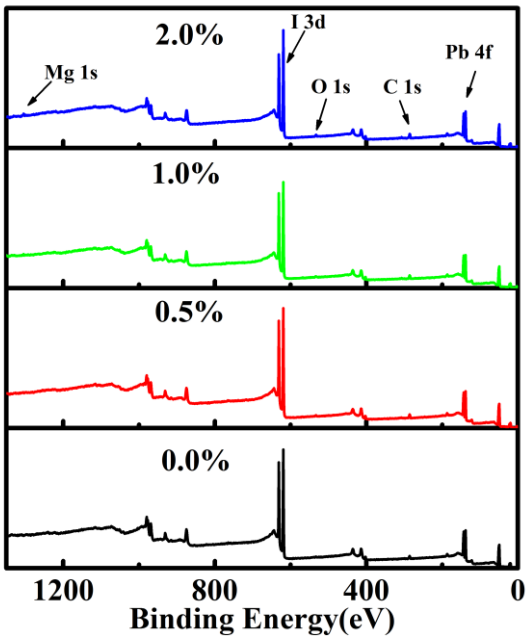

Figure S2 The surface-sensitive XPS spectra of different content MgI_2-doped $MAPbI_3$ perovskite film on FTO glass substrates.

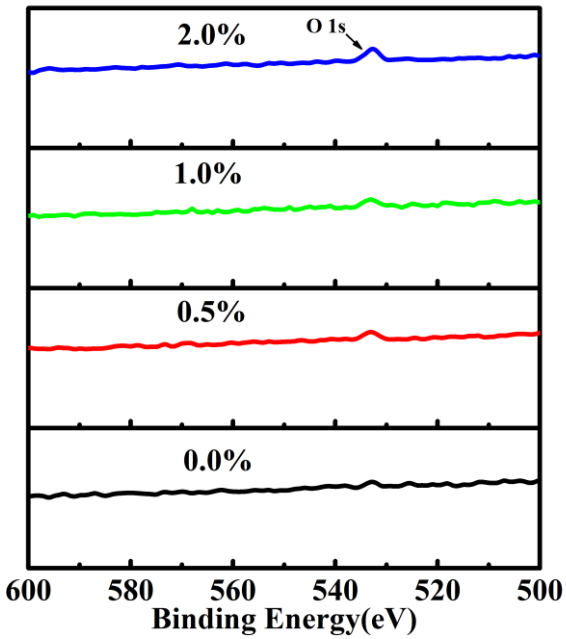

Figure S3 The XPS core level spectra of O 1s.

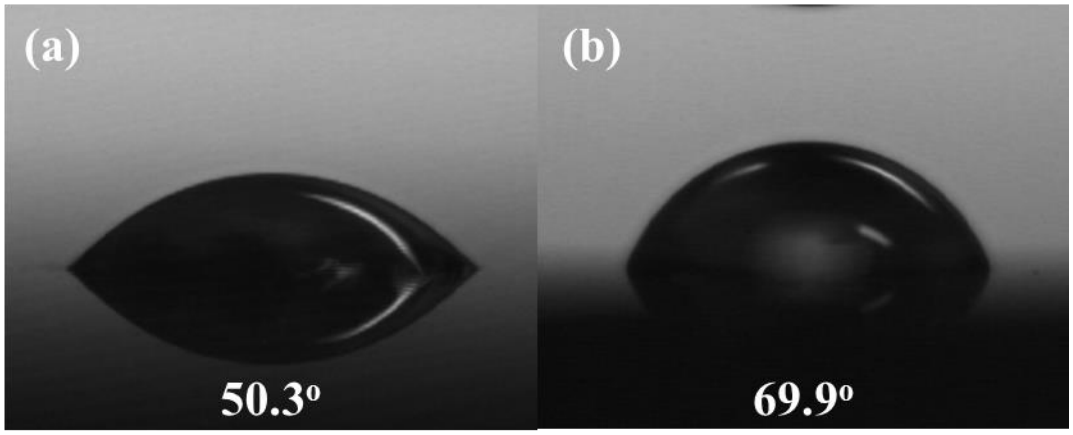

Figure S4 The contact angle between perovskite film and water droplet. (a) Pristine $MAPbI_3$ and (b) 1.0 % MgI_2-doped.

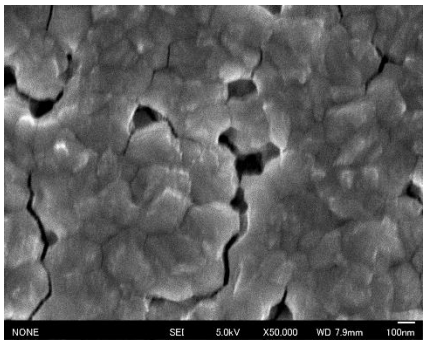

Figure S5 SEM images of the annealed 4% Mg-dopedMAPbI$_3$ perovskite layers on FTO/compact TiO2/mesoporous TiO2 substrate. Scan bar: 100 nm.

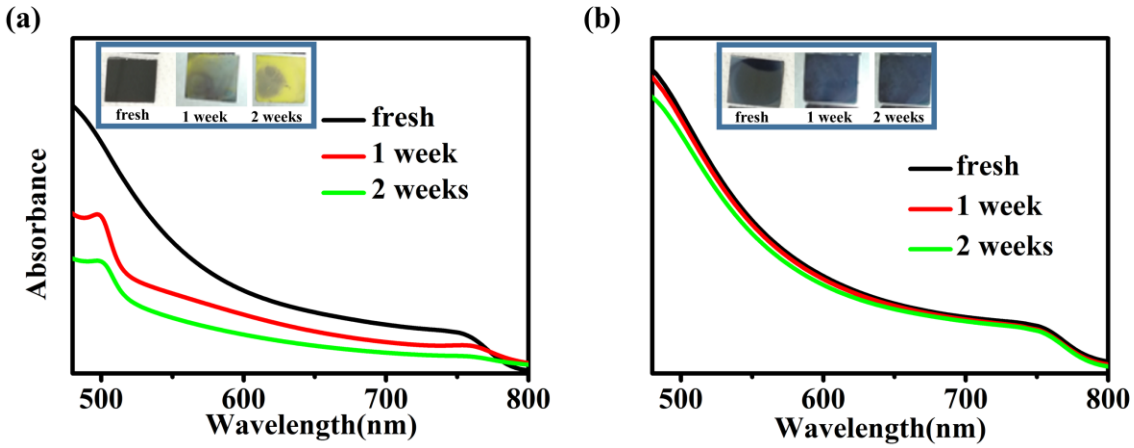

Figure S6 The stability of doping free and 1 % Mg doping perovskite film on the glass substrates. The films were prepared and kept at 30~40% RH atmosphere. The insert is the photograph of the corresponding perovskite films. (a) Doping free perovskite film. (b) 1.0 % Mg doping perovskite film.

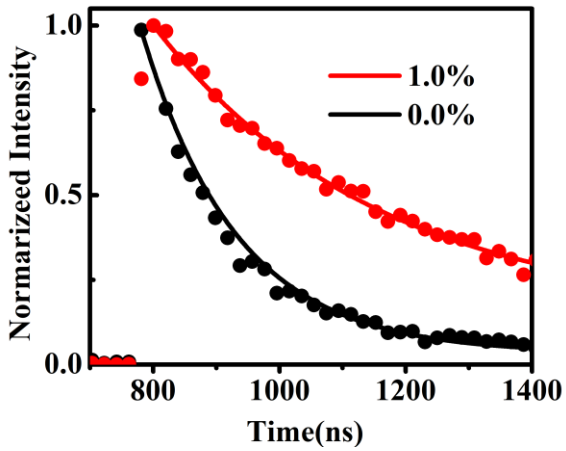

Figure S7 Time-resolved photoluminescence (TRPL) spectra (excitation at 515 nm and emission at 771 nm) of the $MAPbI_3$ perovskite and 1% Mg-doped $MAPbI_3$ film deposited on glass substrates.

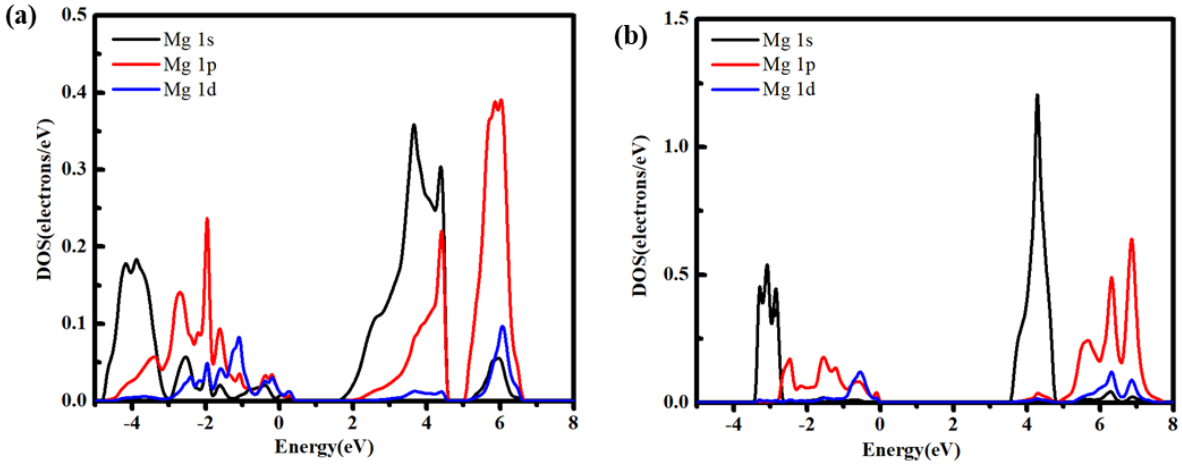

Figure S8 DOS diagrams for (a) $MAMgI_3$ (b) MgI_2

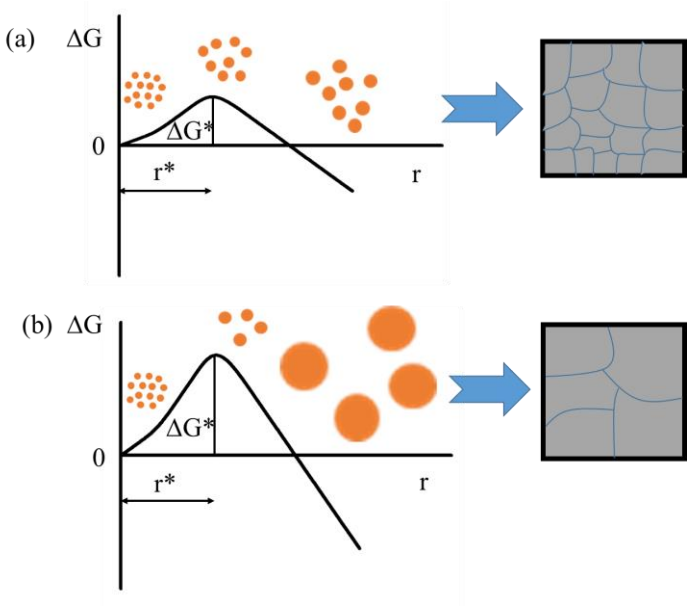

Figure S9 (a) Gibbs free energy diagram for nucleation and growth the pristine MAPbI3 layer, (b) Gibbs free energy diagram for nucleation and growth the Mg doped MAPbI3 layer.

Condition	2θ(deg)	d(Å)
0.0%	14.0785	6.2856
0.5%	14.091	6.2800
1.0%	14.1012	6.2755
2.0%	14.1032	6.2747

Table S1 Detail information of the (110) diffraction peak.